Author Manuscript

Author Manuscript

Author Manuscript

Author Manuscript

HHS Public Access

Author manuscript

J Am Chem Soc. Author manuscript; available in PMC 2020 July 03.

Published in final edited form as:

J Am Chem Soc. 2019 July 03; 141(26): 10361–10371. doi:10.1021/jacs.9b03927.

Molecular Mechanisms of Membrane Curvature Sensing by a Disordered Protein

Wade F. Zeno[a], **Ajay S. Thatte**[a], **Liping Wang**[b], **Wilton T. Snead**[a], **Eileen M. Lafer**[b], and **Jeanne C. Stachowiak**[a,c,*]

[a]Department of Biomedical Engineering, The University of Texas at Austin, Austin, TX 78712;

[b]Department of Biochemistry and Structural Biology, The University of Texas Health Science Center at San Antonio, San Antonio, TX 78229;

[c]Institute for Cellular and Molecular Biology, The University of Texas at Austin, Austin, TX 78712

Abstract

The ability of proteins to sense membrane curvature is essential for the initiation and assembly of curved membrane structures. Established mechanisms of curvature sensing rely on proteins with specific structural features. In contrast, it has recently been discovered that intrinsically disordered proteins, which lack a defined three-dimensional fold, can also be potent sensors of membrane curvature. *How can an unstructured protein sense the structure of the membrane surface?* Many disordered proteins that associate with membranes have two key physical features – a high degree of conformational entropy and a high net negative charge. Binding of such proteins to membrane surfaces results simultaneously in a decrease in conformational entropy and an increase in electrostatic repulsion by anionic lipids. Here we show that each of these effects gives rise to a distinct mechanism of curvature sensing. Specifically, as the curvature of the membrane increases, the steric hindrance between the disordered protein and membrane is reduced, leading to an increase in chain entropy. At the same time, increasing membrane curvature increases the average separation between anionic amino acids and lipids, creating an electrostatic preference for curved membranes. Using quantitative imaging of membrane vesicles, our results demonstrate that long disordered amino acid chains with low net charge sense curvature predominately through the entropic mechanism. In contrast, shorter, more highly charged amino acid chains rely largely on the electrostatic mechanism. These findings provide a roadmap for predicting and testing the curvature sensitivity of the large and diverse set of disordered proteins that function at cellular membranes.

Graphical Abstract

*Correspondence and requests for materials should be addressed to J.C.S. (jcstach@austin.utexas.edu).

AUTHOR CONTRIBUTIONS

All authors designed and performed experiments. In addition, all authors consulted together on the interpretation of results and the preparation of the manuscript.

COMPETING INTERESTS

The authors declare no competing interests.

SUPPORTING INFORMATION

Detailed discussion and calculations regarding polymer models and FRET, protein residue information and primary sequences, and raw data

Author Manuscript Author Manuscript Author Manuscript Author Manuscript

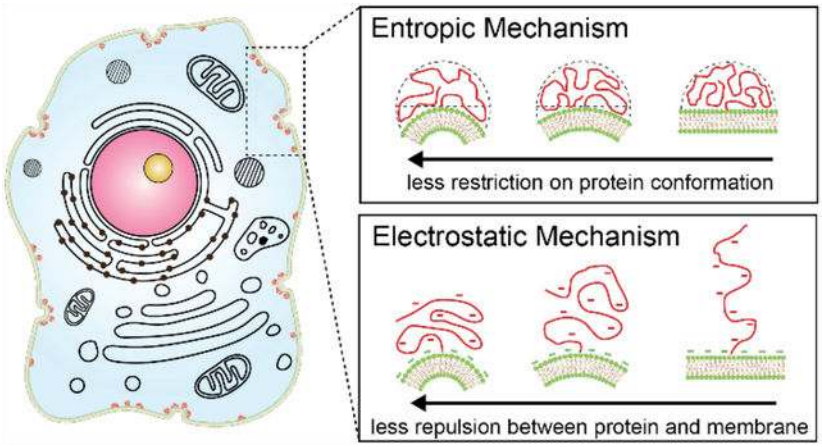

INTRODUCTION

Curved membrane structures such as endocytic pits, viral buds, and tubular organelles play important roles in cellular physiology.[1] Assembly of these structures requires proteins that are capable of sensing and stabilizing membrane curvature.[2, 3] To date, two primary mechanisms of membrane curvature sensing have been widely established, both of which rely on specific structural features. First, amphipathic helices insert into membrane defects, which are found in higher densities in highly curved membrane surfaces.[4].

Second, curved protein scaffolds, such as the crescent-shaped BAR (Bin/Amphiphysin/Rvs) domains,[5] bind more tightly to highly curved membrane surfaces, which match their curvature. Amphipathic helices and curved scaffolds are commonly found within proteins that participate in clathrin-mediated endocytosis[1] and other membrane vesiculation pathways.[6, 7] However, intrinsically disordered domains are also highly abundant within these same proteins.[8–11] Specifically, more than 40% of the proteins involved in membrane traffic contain substantial regions that lack a well-defined three-dimensional structure. These disordered amino acid chains behave more like random polymers than like stably folded domains.[9] Nonetheless, intrinsically disordered domains have been largely neglected in the study of curvature sensing behavior, based on the common assumption that curvature sensing requires specific structural motifs. One example of a disordered protein that has been utilized in previous curvature sensing studies is alpha-synuclein.[12] The curvature sensitivity of this protein is attributed to a direct membrane interaction that induces formation of an amphipathic helix.[13] Disordered domains that do not directly interact with membranes have not been shown to undergo this folding transition. If these types of disordered proteins are able to participate in membrane curvature sensing, then other sensing mechanisms must exist.

Recently we reported that polymer-like disordered domains bind preferentially to small, highly curved vesicles[14]. This finding, which suggests that disordered proteins participate significantly in membrane curvature sensing, is highly significant owing to the abundance of disordered domains in membrane remodeling,[9–11] signaling,[15, 16] and other membraneassociated functions.[17] However, the detailed molecular mechanisms responsible

Author Manuscript Author Manuscript Author Manuscript Author Manuscript

for the ability of disordered domains to sense membrane curvature remain unclear. To probe these mechanisms, here we examine a series of disordered amino acid chains of decreasing length, which consist of truncations of the C-terminal domain of the endocytic protein AP180 (AP180CTD).[14] Importantly, the physical[18, 19] and biochemical[20] properties of AP180CTD have been well-studied, making this protein a good model for understanding the biophysical interactions between disordered proteins and membrane surfaces. For each truncation of AP180CTD, we quantified curvature sensitivity by measuring relative protein binding to substrate-tethered vesicles of increasing diameter.

Our results reveal two mechanisms of curvature sensing by disordered domains. The first mechanism is entropic in nature. Tethering a disordered protein to a membrane surface substantially reduces the protein's conformational entropy. As the membrane surface curves away from the protein, taking on a convex shape, conformational entropy increases. This increase favors protein binding to curved membrane surfaces. Our experiments suggest that this entropic mechanism is the primary driver of curvature sensing by long disordered amino acid chains of low net charge. A second mechanism arises from electrostatic effects. Many disordered proteins, including AP180CTD, have a substantial net negative charge. This net charge results in strong electrostatic repulsion by membrane lipids, which typically have a substantial anionic surface potential.[21, 22]

Because membrane curvature increases the average separation between the disordered protein and the membrane surface, electrostatic repulsion is minimized when disordered proteins bind to highly curved surfaces. Our data suggest that this electrostatic mechanism is the primary driver of curvature sensing by short disordered amino acid chains of high net charge. Importantly, this mechanism differs fundamentally from previously characterized mechanisms that rely on attractive electrostatic interactions to sense membrane curvature.[23] For example, BAR domains, which have a positively charge membrane binding surface, maximize attractive electrostatic interactions with negatively charged membranes by binding to membranes that match their curvature.[5]

Taken together, our results demonstrate that disordered proteins can sense membrane curvature using both entropic and electrostatic mechanisms. More broadly, we show that non-specific physical interactions between disordered proteins and membranes can be just as sensitive to membrane curvature as proteins that contain specialized structural motifs such as curved scaffolds and amphipathic helices.[4, 24] As such, this work provides the necessary tools to discover and characterize novel curvature sensing domains among the many intrinsically disordered proteins that reside at membrane surfaces.

RESULTS AND DISCUSSION

The effect of chain length on membrane curvature sensing.

To probe the mechanisms of curvature sensing by disordered proteins, we measured and compared the curvature sensing properties of a series of truncation mutants of decreasing length, which were derived from the disordered C-terminal domain AP180 (AP180CTD), residues 328–898, *Rattus norvegicus*. The truncation mutants consisted of the full disordered domain (571 amino acids), the first two thirds of the disordered domain, AP180CTD-2/3

Author Manuscript Author Manuscript Author Manuscript Author Manuscript

(381 amino acids), and the first one third of the disordered domain, AP180CTD-1/3 (190 amino acids). To quantify the curvature sensing properties of these proteins, we utilized the tethered vesicle assay depicted in Figure 1a. Here a biotinneutravidin interaction was used to tether small unilamellar vesicles (SUVs) to glass surfaces passivated with polyethylene glycol (PEG) as described previously,[4] see methods section. The diameters of the SUVs ranged from 20 nm to 200 nm, encompassing the curvature of many curved biological membrane structures such as clathrin-coated vesicles, multivesicular bodies, and viral buds.[3] Wild-type, full-length AP180 binds to membranes using interactions between the AP180 N-terminal Homology (ANTH) domain and $PI(4,5)P_2$-containing lipids.[25] However, we wanted to examine the curvature sensitivity of the disordered C-terminal domain in isolation. Therefore to facilitate membrane binding, a 6 residue histidine tag was incorporated into all truncation mutants near their N-termini. To facilitate membrane binding of histidine tags, Ni^{2+}-DGSNTA lipids (1,2-dioleoyl-sn-glycero-3-[(N-(5-amino-1-carboxypentyl)iminodiacetic acid)succinyl]) were incorporated into SUVs. SUVs were tethered to the coverslip surface, incubated with protein-containing solutions, and visualized using fluorescence microscopy.

Using this assay, we compared the curvature sensing properties of AP180CTD and histidine-tagged green fluorescent protein (GFP). Here GFP, which is not expected to have curvature sensing properties, was included to provide a negative control for the study. Figure 1b shows representative images of GFP and AP180CTD binding to separate populations of tethered vesicles. SUVs were fluorescently labeled with the lipid dye, Texas Red-DHPE (1,2-dihexadecanoyl-sn-glycero-3-phosphoethanolamine), while AP180CTD truncation mutants were labeled with ATTO-488, conjugated covalently to a primary amine within each protein. To minimize any quenching of ATTO-488 by Texas-Red via fluorescence resonance energy transfer (FRET), Texas Red-DHPE was incorporated into SUVs at a relatively low concentration of 0.2 mol%. At this concentration the average distance between donor and acceptor fluorophores was more than twice the Förster radius (see Supporting Information). As expected, no significant FRET effect was observed as indicated by the data in Supporting Figure S1. Specifically, GFP and ATTO-488 fluorescence intensity distributions remained nearly identical in the presence and absence of Texas Red-DHPE.

Using the tethered vesicle assay, we examined the partitioning of AP180CTD and GFP among vesicles of varying diameters. In Figure 1b (top row), the ratio of GFP fluorescence intensity in the green channel to lipid fluorescence intensity in the red channel appeared relatively constant across the entire range of SUV diameters, such that SUVs appeared to have a uniform yellow color when the channels were merged. This observation suggests qualitatively that GFP binding is not sensitive to membrane curvature, as expected. In contrast, AP180CTD displayed visible curvature sensitivity in the tethered vesicle assay, Figure 1b, bottom row. Specifically, the ratio of protein fluorescence intensity to lipid fluorescence intensity generally increased as SUV diameter decreased. In this way, smaller SUVs appeared more green while larger SUVs appeared more red in the merged images.

To quantitatively compare curvature sensing by AP180CTD and its truncation mutants, we measured fluorescence intensity of colocalized protein and lipid fluorescence channels to determine the number of proteins bound to each SUV, Figure 1c. The distribution of SUV

Author Manuscript Author Manuscript Author Manuscript Author Manuscript

diameter was estimated by comparing the mean Texas Red-DHPE fluorescence intensity per tethered vesicle to the mean diameter obtained from dynamic light scattering, as described previously[26] and outlined in the methods section. The number of proteins bound to each vesicle was estimated by dividing the fluorescence intensity of each SUV in the protein channel by the calibrated fluorescence intensity of dye-labeled proteins, see methods. For each protein tested, the number of bound proteins increased monotonically as SUV diameter increased, as expected, Figure 1c.

If a protein binds preferentially to membranes of high curvature, the density of membranebound protein, defined as the number of bound proteins per membrane surface area, should increase with decreasing SUV diameter. Therefore, to evaluate curvature sensing behavior, we calculated the relative protein partitioning factor, K_{rel}, as a function of SUV diameter, Figure 1d. Here the value of K_{rel} for SUVs of a particular diameter is defined as the density of protein binding to vesicles of that diameter, divided by the density of protein binding to vesicles of a large reference diameter, 200 nm. For GFP, negligible curvature sensitivity was observed, as K_{rel} remained nearly constant over the entire range of SUV diameter. In contrast, the value of K_{rel} for AP180CTD increased about 8-fold as SUV diameter decreased from 200 nm to 20 nm, indicating substantial sensitivity to membrane curvature. AP180CTD-2/3 and AP180CTD-1/3 exhibited lesser magnitudes of curvature sensitivity, with K_{rel} increasing about 5-fold and 4-fold, respectively, over the same range of SUV diameter. The observed reduction in curvature sensitivity with decreasing chain length is qualitatively consistent with shorter polymer chains having less conformational entropy than longer chains.

K_{rel} represents the probability that a protein will bind to a vesicle of smaller diameter, normalized by the probability of binding to vesicles of the larger reference diameter, 200 nm. If we assume that protein binding is a random, Boltzmann-distributed process, we can use Equation 1 to estimate the decrease in free energy, ΔG_{rel}, associated with protein binding to vesicles of a particular diameter.

$$\Delta G_{rel} = -k_B T \ln\left(K_{rel}\right) \quad (1)$$

Using this approach, Figure 1e plots the values of ΔG_{rel} for binding of each of the AP180CTD truncation mutants to vesicles of 25 nm diameter. The change in ΔG_{rel} with increasing amino acid chain length can help us to understand the physical origins of curvature sensing. Specifically, if curvature sensing arises from the influence of the membrane surface on the entropy of the amino acid chain, then ΔG_{rel} can be approximated as $-T\Delta S_{rel}$. Here ΔS_{rel} is the change in the entropy of the membrane-bound amino acid chain as membrane curvature increases. Importantly, ΔS_{rel} is a relative quantity, which does not depend directly on the absolute entropy of the polymer-like disordered domains. In addition to the chain entropy effect discussed above, this entropy term could also include contributions from changes in the organization of water molecules around membrane-bound proteins. For polymers modeled as self-avoiding random walks, entropy is expected to scale linearly with the number of segments (N), a measure of chain length.[27] Therefore, if

Author Manuscript Author Manuscript Author Manuscript Author Manuscript

curvature sensing arises from changes in conformational entropy, ΔG_{rel} should scale linearly with N as AP180CTD is truncated, as demonstrated previously using Monte Carlo simulations.[14] This prediction is shown by the dashed line in Figure 1e. Interestingly, the measured reduction in ΔG_{rel} with decreasing chain length is substantially weaker than the predicted reduction. This disparity suggests that factors other than chain entropy may contribute to curvature sensing by AP180CTD and its truncation mutants.

One additional factor that could contribute to curvature sensing is AP180CTD's substantial net negative charge and heterogeneous charge distribution, Supporting Table S1. Specifically, as AP180CTD is truncated to AP180CTD-1/3, the average charge per residue nearly doubles, increasing from −0.06 to −0.11. The degree of electrostatic repulsion between these negative charges can be tuned by varying the ionic strength in solution. In the next section, we use this approach to investigate the impact of electrostatic repulsion within the amino acid chain on the hydrodynamic radii of the disordered amino acid chains.

Impact of ionic strength on the hydrodynamic radius of AP180CTD

Here we investigate the effect of electrostatic screening on the hydrodynamic radii of AP180CTD truncation mutants and determine the ability of polymer scaling laws to predict these changes. The extent to which electrostatic interactions are screened can be controlled by varying the ionic strength of the solution, Figure 2a. Therefore we used fluorescence correlation spectroscopy (FCS) to measure the hydrodynamic radii of AP180CTD truncation mutants in solutions of varying ionic strength, Figure 2b–d. The mean time that each protein spent in the diffraction-limited laser focal volume was determined by fitting Equation 2 to the FCS correlation curve, as described in the methods section. This characteristic decay time is directly proportional to the protein radius. For each concentration of sodium chloride in solution, decay time increased as the number of residues in the disordered domain increased, Fig. 2b–d, Supporting Table S2. After accounting for changes in solution viscosity, the hydrodynamic radius of each protein was estimated at each concentration of sodium chloride, Supporting Table S2. These results are summarized in Figure 2e. The hydrodynamic radius of AP180CTD increased by 35% as the concentration of sodium chloride decreased from 1000 mM to 10 mM. In contrast, the hydrodynamic radii of AP180CTD-2/3 and AP180CTD-1/3 each increased by somewhat larger percentages, 51% and 65%, respectively, over the same range of solution conditions.

Using these results, we estimated the effective rigidity of each disordered protein using two metrics: effective rigid segment length, also known as Kuhn length (l_k), and effective number of rigid segments (N). Both metrics are reported as a function of ionic strength in Figure 2f. The details of these calculations are outlined in the Supporting Information. For AP180CTD, l_k increased approximately 2-fold as sodium chloride concentration was reduced from 1000 mM to 10 mM. This result indicates that the protein chain became more rigid as ionic strength was reduced, presumably owing to the associated increase in electrostatic repulsion between anionic amino acids. In this same range of ionic strength, the effective Kuhn lengths of AP180CTD-2/3 and AP180CTD-1/3 increased by larger magnitudes, 2.7-fold and 3.4-fold, respectively. These trends are consistent with AP180CTD-1/3 having the highest charge density and AP180CTD having the lowest charge

Author Manuscript Author Manuscript Author Manuscript Author Manuscript

density, Supporting Table S1. Similarly, as the chain became shorter and more highly charged, the deviation increased between the measured hydrodynamic radii and the radii we would expect from modeling the proteins as self-avoiding walks, as shown in Supporting Figure S2a–c. Collectively these results demonstrate that the physical properties of the disordered amino acid chains are significantly impacted by intra-chain electrostatic interactions. Therefore we next examined the impact of ionic strength on curvature sensing by AP180CTD and its truncation mutants.

Impact of ionic strength on curvature sensing

When disordered proteins are bound to the surface of a membrane, a highly curved membrane surface would be expected to increase the average separation between negatively charged amino acids and negatively charged lipids. This increased separation could drive proteins to bind preferentially to more highly curved membrane surfaces. Importantly, electrophoretic mobility measurements at pH 7.4 revealed that the SUVs used in our curvature sensing experiments, which were composed of 87.8% DOPC, 10% DGS-NTA, 2% DP-EG10-Biotin, and 0.2% Texas Red-DHPE, had a negative zeta potential of −35 + 3 mV. The negative zeta potential likely arose from the negative charge in the nitrilotriacetic acid head group of DGS-NTA. This result suggests that negatively charged proteins could be repelled from the membrane surface.

Interestingly, changes in ionic strength of the solution would be expected to impact electrostatic and entropic curvature sensing mechanisms oppositely. Specifically, increasing the ionic strength in solution buffers electrostatic repulsion, making the amino acid chain more flexible, as demonstrated by the data in Figure 2a. This effect would be expected to increase entropic curvature sensing. In contrast, the same decrease in electrostatic repulsion would be expected to decrease electrostatic curvature sensing. Importantly, these opposing effects provide an opportunity to distinguish between the two sensing mechanisms. Specifically, if increasing ionic strength causes curvature sensitivity to increase, then the entropic mechanism is dominant. In contrast, if decreasing ionic strength causes curvature sensitivity to increase, then the electrostatic mechanism is dominant.

To probe the relative importance of the two mechanisms, we examined the curvature sensitivity of AP180CTD and its truncation mutants as a function of ionic strength. Figure 3a–c reports the results under conditions of strong electrostatic screening, 1000 mM sodium chloride. Under these conditions, GFP exhibited no appreciable curvature sensitivity, as expected, binding at approximately the same density to SUVs with diameters ranging from 20 nm to 200 nm, Figure 3a. In contrast, AP180CTD displayed significant curvature sensitivity with a K_{rel} value of 13.8 on 20 nm SUVs. Lesser degrees of curvature sensitivity were observed for AP180CTD-2/3 and −1/3, with K_{rel} values of 5.9 and 2.9, respectively. Relative to the 150 mM NaCl condition tested in Figure 1d, K_{rel} values increased by 67% for AP180CTD, indicating a substantial increase in curvature sensitivity. This result suggests that curvature sensing by AP180CTD arises primarily from the entropic mechanism, Figure 3b. In contrast, the curvature sensitivity of AP180CTD-1/3 decreased by 25% as the sodium chloride concentration increased from 150 mM to 1000 mM. This result suggests that the proposed electrostatic mechanism dominates curvature sensing by AP180CTD-1/3.

Author Manuscript Author Manuscript Author Manuscript Author Manuscript

Importantly, AP180CTD-1/3 has both the shortest length and the highest charge per residue of the three amino acid chains, Supporting Table S1. Both of these factors would be expected to favor the electrostatic mechanism over the entropic mechanism. Interestingly, AP180CTD-2/3 exhibited no significant change in sensitivity, indicating that the electrostatic and entropic mechanism may be comparable in magnitude for this protein. In Figure 3c, ΔG_{rel} between proteins on 25 nm and 200 nm diameter SUVs was estimated using Equation 1. Unlike the result in Figure 1e, the increase in ΔG_{rel} with increasing amino acid chain length at 1000 mM sodium chloride is in good agreement with the linear scaling predicted by the self-avoiding walk model, dashed line. This result suggests that electrostatic interactions between amino acid residues are thoroughly screened, such that each truncation mutant has approximately the same flexibility, despite their differing concentrations of charged residues.

We next examined the curvature sensitivity of AP180CTD and its truncation mutants under conditions of low electrostatic screening, 10 mM sodium chloride, where the electrostatic mechanism would be expected to have its greatest effect, Figure 3d–f. Vesicles were composed of 87.8% DOPC, 10% DGS-NTA, 2% DP-EG10-Biotin, and 0.2% Texas Red-DHPE. The negative SUV charge arose from the negative charges in the head groups of the DGS-NTA lipids. Notably, even GFP exhibited significant curvature sensitivity under these conditions, with a K_{rel} value of about 2.5 for 20 nm SUVs, Figure 3d. We attribute this result to GFP having a net negative charge of approximately 8 in the experimental buffer, which had a pH of 7.4. The isoelectric point of GFP is approximately 5.6.[28] The reduction in sodium chloride concentration from 150 mM to 10 mM also impacted curvature sensing by the disordered amino acid chains, resulting in a 29% decrease in sensing by AP180CTD, as shown in Figure 3e. Interestingly, the curvature sensitivity of AP180CTD-1/3 increased by 84% when the concentration of sodium chloride was reduced from 150 mM to 10 mM, further suggesting that the electrostatic mechanism of curvature sensing is the dominant mechanism for this protein. Though the curvature sensitivity of AP180CTD-2/3 increased by an average value of 26% over the same change in sodium chloride concentration, we found this change to be statistically nonsignificant. This result further suggests that the entropic and electrostatic mechanisms have comparable impact on curvature sensing by AP180CTD-2/3.

Interestingly, curvature sensing by AP180CTD and its truncation mutants is not highly sensitive to amino acid chain length in the low ionic strength regime (Fig. 3f), suggesting that the electrostatic mechanism lacks a strong dependence on chain length. To understand this result, we considered the impact of increasing chain length on the net electrostatic repulsion of the amino acid chain from the membrane surface. Specifically, as the chain length increases, the net charge of the disordered protein increases, an effect which would be expected to increase electrostatic repulsion from the charged membrane. However, the average separation between charges in the amino acid chain and charges on the membrane surface also increases with increasing chain length, owing to the increased hydrodynamic radius of the longer amino acid chain, Figure 2e. These two effects would be expected to have opposite impacts on the net electrostatic repulsion between the amino acid chain and the membrane surface. Therefore, it is not surprising that the electrostatic curvature sensing effect scales only weakly with chain length. The slight increase in curvature sensitivity that

Author Manuscript Author Manuscript Author Manuscript Author Manuscript

we observe as chain length decreases (Fig. 3f) likely arises from the greater concentration of charged amino acids in the shorter truncation mutants (Supporting Table S1).

Taken together, the variation in curvature sensing as a function of ionic strength illustrates that disordered proteins can sense membrane curvature by at least two distinct mechanisms. In the limit of a long amino acid chain and strong screening of electrostatic interactions between the chain and the membrane surface, curvature sensing arises primarily from the fact that the more highly curved the membrane surface becomes, the less it restricts the conformational entropy of the amino acid chain, Figure 4a. This is the entropically controlled regime of curvature sensing, as observed with AP180CTD in Figure 4b. In contrast, as the chain takes on a higher net charge and the extent of electrostatic screening is decreased, we enter a regime in which curvature sensing appears to arise from electrostatic repulsion between the amino acid chain and the membrane surface. Here electrostatic repulsion is minimized when the membrane curves away from the chain, resulting in stronger binding to more highly curved membrane surfaces, Figure 4c. This is the electrostatically controlled regime of curvature sensing, as observed with AP180CTD-1/3 in Figure 4d. For AP180CTD-2/3, the entropic and electrostatic curvature sensing mechanisms seem to have approximately equivalent significance, resulting in a nearly constant sensitivity to membrane curvature over the range of ionic strengths we examine, Figure 4e

Impact of surface charge on curvature sensing

If electrostatic repulsion between membrane lipids and charged amino acids can give rise to curvature sensing, then increasing the concentration of negatively charged lipids should drive an increase in curvature sensitivity. To test this prediction, we incorporated the anionic lipid, DOPS (1,2-dioleoyl-sn-glycero-3-phospho-L-serine), into our liposomes. Relative to pure DOPC, the addition of DGS-NTA, DP-EG10-Biotin, and Texas Red-DHPE increased the magnitude of the zeta potential of the liposomes from 20 mV to 35 mV, Figure 5a. The magnitude of the liposomal zeta potential of the liposomes increased by an additional 40% as the mole fraction of DOPS increased from 0% to 2%. As expected, curvature sensitivity increased for all disordered proteins as DOPS content increased, Figure 5b–d. Values of the relative partitioning coefficient, K_{rel}, increased proportionally as expected, Figure 5e. These increases were greatest for AP180CTD-1/3, consistent with its higher charge density, Supporting Table S1. Interestingly, even for AP180CTD, where entropic curvature sensing appears to dominate, Figure 4b, adding DOPS lipids to the membrane resulted in increased curvature sensitivity, Figure 5d. This finding illustrates that the electrostatic mechanism of curvature sensing can work together with the entropic mechanism to enhance overall curvature sensitivity.

CONCLUSIONS

Here we demonstrate that an intrinsically disordered protein, the C-terminal domain of AP180,[14, 18–20] can sense membrane curvature using two distinct mechanisms. The first is entropic in nature. Here the disordered protein maximizes its conformational entropy by binding to highly curved membrane surfaces. The second mechanism arises from electrostatic repulsion between the disordered domain and the membrane surface, both of

Author Manuscript Author Manuscript Author Manuscript Author Manuscript

which carry a substantial net negative charge. Here electrostatic repulsion drives disordered domains to partition preferentially to highly curved surfaces, which increase the separation between anionic amino acids and membrane lipids. The entropic mechanism requires disordered domains to be long, while the electrostatic mechanism is relatively independent of amino acid chain length. Together these results could explain curvature sensing for many different disordered domains over a broad range of length, charge density, and ionic strength.

Curvature sensing is an advantageous feature for proteins involved in membrane remodeling because it allows proteins to efficiently partition into regions of high curvature. Once a sufficiently high concentration of membrane-bound protein is reached, membrane deformation can be induced via mechanisms such as protein crowding.[19, 29] Many disordered proteins that interact with membrane surfaces are involved in membrane remodeling. A few examples include disordered domains that are components of G protein-coupled receptors (GPCRs),[15, 17] are involved in actin binding,[30, 31] or are part of the structure of the immunological synapse,[32, 33] among many others. In principle, any of these disordered domains could sense membrane curvature. Future work has the potential to develop a predictive understanding of curvature sensing. While the present work provides simple mechanistic arguments, a predictive understanding requires models that take into account the specific amino acid sequences of disordered domains and the characteristics of the membrane surface. This modeling could be accomplished using coarse-grained simulation methods that have previously been applied to charged polymers.[34, 35] Experimentally, charge distributions within disordered domains can be modified by site-directed mutagenesis or phosphorylation to further examine the effects of charge density on curvature sensitivity.

This work demonstrates that disordered proteins can sense membrane curvature using multiple, highly-potent mechanisms, despite their lack of secondary or tertiary structure. Specifically, our results demonstrate that disordered domains can have a 3 to 14 fold preference for highly curved membrane surfaces, relative to flat ones. This level of sensitivity is comparable to previous reports for structured curvature sensors such as NBAR domains[5, 24] and amphipathic helices from diverse proteins involved in membrane traffic.[4, 24, 3637] Based on these findings, it appears likely that disordered domains, which are thought to comprise about one third of the proteome,[38] represent a large and diverse group of potential curvature sensors that remain to be characterized.

MATERIALS AND METHODS

Materials

DOPC (1,2-dioleoyl-sn-glycero-3-phosphocholine), DOPS (1,2-dioleoyl-sn-glycero-3-phospho-L-serine), and DGS-NTA (1,2-dioleoyl-sn-glycero-3-[(N-(5-amino-1-carboxypentyl)iminodiacetic acid)succinyl] nickel salt) were purchased from Avanti Polar Lipids, Inc. DP-EG10-biotin (dipalmitoyl-decaethylene-glycol-biotin) was generously provided by Darryl Sasaki from Sandia National Laboratories, Livermore, CA.[39] Texas Red-DHPE (Texas Red- 1,2-dihexadecanoyl-sn-glycero-3-phosphoethanolamine triethylammonium salt),NeutrAvidin, and Zeba spin desalting columns (7K MWCO, 5 mL) were purchased from Thermo Fisher Scientific. TCEP (Tris(2-carboxyethyl) phosphine

Author Manuscript Author Manuscript Author Manuscript Author Manuscript

hydrochloride), PMSF (phenylmethanesulfonyl fluoride), EDTA-free protease inhibitor tablets, imidazole, PLL (poly-L-lysine), and ATTO-488 NHS-ester, and Thrombin CleaveCleave Kit were purchased from Sigma-Aldrich. Sodium chloride, HEPES (4–2(2-hydroxymethyl)-1-piparazineethanesulphonic acid), IPTG (isopropyl-β-D-thiogalactopyranoside), β-mercaptoethanol, and Triton X-100 were purchased from Fisher Scientific. Amine reactive PEG (mPEG-Succinimidyl Valerate MW 5000) and PEGbiotin (Biotin-PEG SVA MW 5000) were purchased from Laysan Bio, Inc. Transferrin (Human Apo-Transferrin) was purchased from R&D Systems, Inc. Glutathione Sepharose 4B was purchased from GE Healthcare. Amicon Ultra-15 centrifugal filter units were purchased from MilliporeSigma. All reagents were used without additional purification.

Plasmids for AP180CTD constructs

The DNA plasmid for AP180CTD (rat AP180, amino acids 328–898; CAA48748) in a pET32c vector was kindly provided by Ernst Ungewickell, Hannover Medical School, Germany. DNA coding for histidine-tagged AP180CTD was cloned into a pGex4T2 vector as previously described.[19] Constructs coding for AP180CTD-1/3 and AP180CTD-2/3 were developed by performing site-directed mutagenesis on the AP180CTD construct. To generate the AP180CTD-1/3 construct, the AP180CTD plasmid was PCR amplified using primers that introduced a premature stop codon (TAA) in place of the codon for alanine at position 213 (Supporting Fig. S3 and Supporting Table S3). For AP180CTD-2/3, PCR primers introduced a premature stop codon (TGA) in place of the codon for serine at position 414 (Supporting Fig. S3 and Supporting Table S3).

Protein Expression and Purification

AP180CTD-1/3, −2/3, and –FL were each expressed as fusion proteins with an N-terminal GST tag for increased stability. GST was subsequently removed by thrombin cleavage. AP180CTD plasmids were transformed into E. coli BL21 competent cells (NEB cat#2530H), which were grown at 30°C until the suspension reached an OD_{600} of 0.8. Protein expression was induced with 1 mM IPTG for 7 hours at 30°C. Cells were pelleted and stored in −70°C. The whole protein purification was performed at 4°C. Cells were resuspended in lysis buffer [0.5 M Tris pH 8.0, 5 mM EDTA, 5 v/v% glycerol, 5 mM TCEP (GOLDBIO cat# TCEP25), and Roche protease inhibitor cocktail (Roche cat#05056489001) pellets 1/50ml]. The suspension was sonicated on ice (4 × 2000 joules) and 1 v/v% Triton X-100 was added to the lysate. The mixture was clarified by ultracentrifugation at 186,010 × g for 30 minutes, and the supernatant was chromatographed on a glutathione sepharose column. GST-containing proteins were eluted from the column with 15 mM glutathione in lysis buffer, and exchanged into 50 mM Tris, 10 mM $CaCl_2$ (pH 8.0) using a Zeba Desalting Column (Thermo Scientific cat#89891). GST was cleaved using the Thrombin CleanCleave kit (Sigma-Aldrich cat#RECOMT) for 14 hours at 4°C. The cleaved GST was removed with another glutathione sepharose column. Purified protein was then concentrated using an Amicon Ultra-15 centrifugal filter (MilliporeSigma cat# Z740204–24EA) and stored as liquid nitrogen pellets at −80°C.

GFP was prepared as previously described.[40] Briefly, non-dimerizable histidine-tagged EGFP A206K (GFP; AAB02574) was expressed in *E. coli* BL21 (DE3) PlysS cells

Author Manuscript Author Manuscript Author Manuscript Author Manuscript

(Invitrogen). Bacterial lysates were incubated with Ni-NTA agarose in 20 mM HEPES, 150 mM NaCl (pH=7.4) buffer, washed thoroughly, and eluted using the same buffer, but with the addition of 200 mM imidazole. The protein solution was then dialyzed to remove the excess imidazole. Protein was then concentrated, divided into aliquots, frozen in liquid nitrogen, and stored at −80°C.

Protein Labeling

ATTO-488 NHS-ester was dissolved in dimethyl sulfoxide (DMSO) at a concentration of 10 mM and stored at 80°C. Primary amines within AP180CTD derived proteins were then labeled in buffer consisting of 25 mM HEPES, 150 mM NaCl, and 5 mM TCEP (pH = 7.4). Protein concentration varied from 30–80 μM. The dye solution in DMSO was added to the protein solution at a stoichiometric ratio of 2 dye molecules per protein molecule, and allowed to react for 30 minutes at room temperature. The total amount of DMSO present never exceeded 1 v/v%. Labeling ratios for the proteins varied from 0.8 to 1.5 dyes per protein. Unreacted dye was removed using Centri-Spin size exclusion columns (Princeton Separations). Protein and dye concentrations were measured using UV-Vis spectroscopy, and labelled proteins were stored at −80°C.

Preparation of Small Unilamellar Vesicles (SUVs)

Lipid aliquots stored in chloroform at −80°C were brought to room temperature and combined to create lipid mixtures with the appropriate molar ratios. Chloroform was evaporated using a gentle nitrogen stream and the resulting lipid film was further dried under vacuum for at least 2 hours. The lipid film was then hydrated to a total lipid concentration of 200 μM in buffer containing 25 mM HEPES (pH=7.4). The NaCl concentration in this buffer was 10 mM for low ionic strength experiments, 150 mM for medium ionic strength experiments, and 1000 mM for high ionic strength experiments. Rehydrated lipid suspensions were thoroughly mixed and held at room temperature for 15 minutes before sonication and extrusion. The lipid suspension was sonicated in an ice bath using a probe tip sonicator (Branson Ultrasonics). The lipid suspension was extruded through a 100 nm polycarbonate membrane (Whatman plc). Sonication and extrusion yielded SUV populations with average diameters of 50 nm and 115 nm, respectively, as determined by dynamic light scattering.

Tethering of Lipid Vesicles and Protein Binding

Imaging wells consisted of 0.8 mm thick silicone gaskets (Grace Bio-Labs) placed directly on top of no. 1.5 glass coverslips. Polyethylene glycol (PEG) (5 kDa) was conjugated to poly-L-lysine (PLL) via an amine-reactive succinimidyl valeric acid (SVA) group on PEG and primary amines in PLL. PLL-PEG was then used to passivate the glass coverslips. Approximately 2% of the 5 kDa PEG contained a covalently attached biotin group. After 20 minutes of incubation, excess PLL-PEG was rinsed from the wells with a sample buffer containing 25 mM HEPES and 150 mM sodium chloride (pH 7.4). Wells were then incubated with 0.2 mg/mL NeutrAvidin (Thermo Fisher) in the same sample buffer for 10 minutes. Excess NeutrAvidin was then rinsed away using sample buffer that contained the appropriate concentration of sodium chloride (i.e. low, medium, and high ionic strength conditions). Sonicated and extruded SUVs were combined and then added to wells. Higher

Author Manuscript Author Manuscript Author Manuscript Author Manuscript

ionic strengths resulted in reduced binding efficacy of SUVs. Therefore, to maintain adequate tethering density, it was necessary to increase the concentration of SUVs. The lipid concentrations were determined empirically. The respective concentrations of sonicated and extruded SUVs (in terms of total lipid concentration) were as follows: 0.25 μM and 0.75 μM for low ionic strength conditions (10 mM NaCl), 0.5 μM and 1 μM for medium ionic strength conditions (150 mM NaCl), and 2 μM and 20 μM for high ionic strength conditions (1000 mM NaCl). After 10 minutes of incubation, excess SUVs were rinsed from the wells in the appropriate sample buffer and protein-containing solution was added. All samples were incubated with protein-containing solution for at least 20 minutes before being imaged.

Fluorescence Microscopy

Tethered SUVs and membrane-bound proteins were visualized using spinning disc confocal microscopy (Zeiss Axio Observed Z1 with Yokagawa CSU-X1M). Lasers with wavelengths of 488 nm and 561 nm were used for excitation. Emission filters were centered at 525 nm and 629 nm with 50 nm and 62 nm widths, respectively. The system was equipped with a triple pass dichroic mirror (405/488/561 nm), a Plan-Apochromat 100× 1.4 N.A. oil immersion objective, and a cooled (−70°C) EMCCD iXon3 897 camera (Andor Technology; Belfast, UK).

Image Processing

Image stacks were acquired in the direction perpendicular to the plane occupied by the tethered SUVs (16 slices, 0.1 μm steps). The brightest frame of the image stack was chosen as the plane of focus. The vast majority of SUVs appeared as diffraction-limited puncta. The diffraction-limited puncta were fit to two-dimensional Gaussian functions using publicly–available particle detection software (cmeAnalysis).[41] Puncta above the diffraction limit were excluded from the analysis. Amplitudes of Gaussian fits were obtained in both the lipid and protein fluorescent channels. Only puncta with amplitudes significantly above the local fluorescence background were included in our analysis. The program used an algorithm to find puncta in the fluorescent protein channel that were spatially colocalized with centroids of the puncta in the fluorescent lipid channel. The radius of this search region was equal to three times the standard deviation of the Gaussian fit. To further ensure that reported lipid puncta were above noise threshold of our images, we only accepted puncta that persisted in the same location throughout three consecutive frames in the image stack.

Calibration of Vesicle Size and Protein Number

SUV diameter and the number of proteins bound to each SUV were calibrated as previously described.[4, 14] Briefly, SUV diameter was calibrated using SUVs that were extruded (100 nm polycarbonate membrane) and tethered in the absence of protein. The fluorescence intensity distribution for tethered SUVs was obtained using cmeAnalysis. We then computed a scaling factor that centered the peak of the SUV fluorescence intensity distribution to the average SUV diameter obtained from dynamic light scattering. The number of proteins bound to a single vesicle was determined using single molecule imaging. For calibration measurements, proteins were in stoichiometric excess to ATTO 488. This excess ensured that very few proteins were labeled by more than one fluorophore. Proteins were adsorbed to glass cover slips and appeared as diffractionlimited puncta. The fluorescence intensity

Author Manuscript Author Manuscript Author Manuscript Author Manuscript

distribution of adsorbed proteins was acquired using cmeAnalysis. These fluorescence intensity distributions contained one prominent maximum peak, which corresponded to the brightness of a single ATTO-488 molecule or a single GFP. Raw data for protein number and vesicle diameter are shown in Supporting Figures S4–S5.

Zeta Potential Measurements

SUVs were prepared as described in the "Preparation of Small Unilamellar Vesicles" section, using extrusion with 100 nm polycarbonate membranes and a buffer containing 2 mM HEPES and 5 mM sodium chloride (pH = 7.4). After extrusion, SUVs were diluted from a lipid concentration of 200 μM to 10 μM in the same buffer. For each lipid composition, approximately 1 mL of diluted SUV solution was injected into a folded capillary zeta cell (Malvern Panalytical Inc. cat#DTS1070). Zeta potentials were then measured using a Malvern ZetaSizer Nano ZS (Malvern Instruments). At least 36 measurements were recorded for each lipid composition.

Fluorescence Correlation Spectroscopy

As a means of estimating the hydrodynamic radii of the disordered protein domains, fluorescence correlation spectroscopy (FCS) measurements were taken in solution using a custom-built confocal microscope (Zeiss Axio Observer. A1) that has been described previously.[42] This microscope was equipped with a 488 nm picosecond pulsed laser and a time-correlated single photon counting electronic card (Becker and Hickl). Imaging wells were coated with lipid bilayers consisting of 100% DOPC to prevent adsorption of protein from solution. SUVs were prepared via sonication in buffer containing 25 mM HEPES buffer (pH=7.4). The concentration of NaCl was 10 mM for low ionic strength conditions, 150 mM for medium ionic strength conditions, and 1000 mM for high ionic strength conditions. SUVs were added directly to imaging wells and allowed to incubate for at least 10 minutes at room temperature before rinsing and addition of proteins. Protein was added to the well at a concentration of 2 nM. Measurements were taken 3 μm above the glass cover slip. Correlation curves were collected using Becker and Hickl data acquisition software. Curves were fit using a standard 2-dimensional autocorrelation function (Equation 2, Supporting Figs. S6–S7). N_p and τ_D correspond to the number of proteins and protein diffusion time, respectively. An anomalous diffusion exponent, α, was used to improve the quality of the fit. Values for α varied between 0.9–1.0 for all proteins (Supporting Table S2). A and τ_c are variables corresponding to the triplet-state and were held constant at 0.05 and 5 μs, respectively.[43] A, τ_c, and α had negligible impact on the τ_D, which was the regression parameter of interest.

$$G(t) = 1 + \left(1 + Ae^{\frac{t}{T_C}}\right)\left(\frac{1}{N_p}\right)\left(\frac{1}{1 + \left(\frac{t}{T_D}\right)^{\alpha}}\right) \quad (2)$$

Author Manuscript Author Manuscript Author Manuscript Author Manuscript

Calibration of the focal volume width and determination of protein size was accomplished using previously described methods[14], using Green Fluorescent Protein (GFP) and Transferrin as calibration standards of known diameter (Supplementary Fig. S6). These methods were also used to account for variation in solution viscosity as a function of NaCl concentration (Supporting Table S2).

Supplementary Material

Refer to Web version on PubMed Central for supplementary material.

ACKNOWLEDGEMENTS

This research was supported by the National Institutes of Health through R01GM120549 to Stachowiak and Lafer and through F32GM128316 to Zeno. The authors thank Dr. Carl Hayden for advice on the image analysis and the interpretation of spectroscopic data. Purification of AP180CTD and its truncation mutants was performed in the University of Texas Health Science Center at San Antonio Center for Macromolecular Interactions, which is supported by the Mays Center through the National Cancer Institute P30 Grant CA054174, and Texas State funds provided through the UTHSCSA Office of the Vice President for Research.

REFERENCES

(1). McMahon HT; Gallop JL, Membrane curvature and mechanisms of dynamic cell membrane remodelling. Nature 2005, 438, 590–596. [PubMed: 16319878]

(2). Stachowiak JC; Brodsky FM; Miller EA, A cost-benefit analysis of the physical mechanisms of membrane curvature. Nat. Cell Biol 2013, 15, 1019–27. [PubMed: 23999615]

(3). Hurley JH; Boura E; Carlson L-A; Różycki B, Membrane budding. Cell 2010, 143, 875–887. [PubMed: 21145455]

(4). Hatzakis NS; Bhatia VK; Larsen J; Madsen KL; Bolinger P-Y; Kunding AH; Castillo J; Gether U; Hedegård P; Stamou D, How curved membranes recruit amphipathic helices and protein anchoring motifs. Nat. Chem. Biol 2009, 5, 835–841. [PubMed: 19749743]

(5). Peter BJ; Kent HM; Mills IG; Vallis Y; Butler PJG; Evans PR; McMahon HT, BAR domains as sensors of membrane curvature: the amphiphysin BAR structure. Science 2004, 303, 495–499. [PubMed: 14645856]

(6). Lee MC; Orci L; Hamamoto S; Futai E; Ravazzola M; Schekman R, Sar1p N-terminal helix initiates membrane curvature and completes the fission of a COPII vesicle. Cell 2005, 122, 605–617. [PubMed: 16122427]

(7). Farsad K; Ringstad N; Takei K; Floyd SR; Rose K; De Camilli P, Generation of high curvature membranes mediated by direct endophilin bilayer interactions. J. Cell Biol 2001, 155, 193–200. [PubMed: 11604418]

(8). Dyson HJ; Wright PE, Intrinsically unstructured proteins and their functions. Nat. Rev. Mol. Cell Biol 2005, 6, 197–208. [PubMed: 15738986]

(9). Pietrosemoli N; Pancsa R; Tompa P, Structural disorder provides increased adaptability for vesicle trafficking pathways. PLoS Comput. Biol 2013, 9, e1003144. [PubMed: 23874186]

(10). Dafforn TR; Smith CJ, Natively unfolded domains in endocytosis: hooks, lines and linkers. EMBO Rep 2004, 5, 1046–1052. [PubMed: 15520805]

(11). Owen DJ; Collins BM; Evans PR, Adaptors for clathrin coats: structure and function. Annu. Rev. Cell Dev. Biol 2004, 20, 153–91. [PubMed: 15473838]

(12). Jensen MB; Bhatia VK; Jao CC; Rasmussen JE; Pedersen SL; Jensen KJ; Langen R; Stamou D, Membrane Curvature Sensing by Amphipathic Helices a single liposome study using α-synuclein and annexin B12. J. Biol. Chem 2011, 286, 42603–42614. [PubMed: 21953452]

(13). Bartels T; Ahlstrom LS; Leftin A; Kamp F; Haass C; Brown MF; Beyer K, The N-terminus of the intrinsically disordered protein α-synuclein triggers membrane binding and helix folding. Biophys. J 2010, 99, 2116–2124. [PubMed: 20923645]

Author Manuscript Author Manuscript Author Manuscript Author Manuscript

(14). Zeno WF; Baul U; Snead WT; DeGroot AC; Wang L; Lafer EM; Thirumalai D; Stachowiak JC, Synergy between intrinsically disordered domains and structured proteins amplifies membrane curvature sensing. Nat. Commun 2018, 9, 4152. [PubMed: 30297718]

(15). Wright PE; Dyson HJ, Intrinsically disordered proteins in cellular signalling and regulation. Nat Rev Mol Cell Biol 2015, 16, 18. [PubMed: 25531225]

(16). Iakoucheva LM; Brown CJ; Lawson JD; Obradović Z; Dunker AK, Intrinsic disorder in cell-signaling and cancer-associated proteins. J. Mol. Biol 2002, 323, 573–584. [PubMed: 12381310]

(17). Minezaki Y; Homma K; Nishikawa K, Intrinsically disordered regions of human plasma membrane proteins preferentially occur in the cytoplasmic segment. J. Mol. Biol 2007, 368, 902–913. [PubMed: 17368479]

(18). Kalthoff C; Alves J; Urbanke C; Knorr R; Ungewickell EJ, Unusual structural organization of the endocytic proteins AP180 and epsin 1. J. Biol. Chem 2002, 277, 8209–8216. [PubMed: 11756460]

(19). Busch DJ; Houser JR; Hayden CC; Sherman MB; Lafer EM; Stachowiak JC, Intrinsically disordered proteins drive membrane curvature. Nat. Commun 2015, 6, 7875. [PubMed: 26204806]

(20). Zhuo Y; Ilangovan U; Schirf V; Demeler B; Sousa R; Hinck AP; Lafer EM, Dynamic interactions between clathrin and locally structured elements in a disordered protein mediate clathrin lattice assembly. J. Mol. Biol 2010, 404, 274–290. [PubMed: 20875424]

(21). Van Meer G; Voelker DR; Feigenson GW, Membrane lipids: where they are and how they behave. Nat. Rev. Mol. Cell Biol 2008, 9, 112. [PubMed: 18216768]

(22). Sun Y; Drubin DG, The functions of anionic phospholipids during clathrinmediated endocytosis site initiation and vesicle formation. J. Cell Sci 2012, 125, 6157–6165. [PubMed: 23097040]

(23). Antonny B, Mechanisms of membrane curvature sensing. Annu. Rev. Biochem 2011, 80, 101–123. [PubMed: 21438688]

(24). Bhatia VK; Madsen KL; Bolinger PY; Kunding A; Hedegård P; Gether U; Stamou D, Amphipathic motifs in BAR domains are essential for membrane curvature sensing. EMBO J 2009, 28, 3303–3314. [PubMed: 19816406]

(25). Miller S; Mathiasen S; Bright N; Pierre F; Kelly B; Kladt N; Schauss A; Merrifield C; Stamou D; Honing S; Owen D, CALM Regulates Clathrin-Coated Vesicle Size and Maturation by Directly Sensing and Driving Membrane Curvature. Dev. Cell 2015, 33, 163–175. [PubMed: 25898166]

(26). Kunding AH; Mortensen MW; Christensen SM; Stamou D, A fluorescencebased technique to construct size distributions from single-object measurements: application to the extrusion of lipid vesicles. Biophys. J 2008, 95, 1176–1188. [PubMed: 18424503]

(27). Phillips R; Kondev J; Theriot J; Garcia H Physical biology of the cell; Garland Science: New York, U.S.A., 2012.

(28). Gasteiger E; Hoogland C; Gattiker A; Wilkins MR; Appel RD; Bairoch A The proteomics protocols handbook; Springer: New York, U.S.A., 2005.

(29). Snead WT; Zeno WF; Kago G; Perkins RW; Richter JB; Zhao C; Lafer EM; Stachowiak JC, BAR scaffolds drive membrane fission by crowding disordered domains. J. Cell Biol 2019, 218, 664–682. [PubMed: 30504247]

(30). Li P; Banjade S; Cheng H-C; Kim S; Chen B; Guo L; Llaguno M; Hollingsworth JV; King DS; Banani SF; Russo PS; Jiang Q-X; Nixong BT; Rosen MK, Phase transitions in the assembly of multivalent signalling proteins. Nature 2012, 483, 336–340. [PubMed: 22398450]

(31). Banjade S; Rosen MK, Phase transitions of multivalent proteins can promote clustering of membrane receptors. eLife 2014, 3, e04123.

(32). Kim E; Sheng M, PDZ domain proteins of synapses. Nat. Rev. Neurosci 2004, 5, 771. [PubMed: 15378037]

(33). Buday L; Tompa P, Functional classification of scaffold proteins and related molecules. FEBS J 2010, 277, 4348–4355. [PubMed: 20883491]

(34). Samanta HS; Chakraborty D; Thirumalai D, Charge fluctuation effects on the shape of flexible polyampholytes with applications to intrinsically disordered proteins. J. Chem. Phys 2018, 149, 163323. [PubMed: 30384718]

Author Manuscript Author Manuscript Author Manuscript Author Manuscript

(35). Baul U; Chakraborty D; Mugnai ML; Straub JE; Thirumalai D, Sequence effects on size, shape, and structural heterogeneity in Intrinsically Disordered Proteins. bioRxiv 2018, 427476.

(36). Capraro BR; Yoon Y; Cho W; Baumgart T, Curvature sensing by the epsin N-terminal homology domain measured on cylindrical lipid membrane tethers. J. Am. Chem. Soc 2010, 132, 1200–1201. [PubMed: 20050657]

(37). Drin G; Casella J-F; Gautier R; Boehmer T; Schwartz TU; Antonny B, A general amphipathic α-helical motif for sensing membrane curvature. Nat. Struct. Mol. Biol 2007, 14, 138. [PubMed: 17220896]

(38). Ward JJ; Sodhi JS; McGuffin LJ; Buxton BF; Jones DT, Prediction and functional analysis of native disorder in proteins from the three kingdoms of life. J. Mol. Biol 2004, 337, 635–645. [PubMed: 15019783]

(39). Momin N; Lee S; Gadok A; Busch D; Bachand G; Hayden C; Stachowiak J; Sasaki D, Designing lipids for selective partitioning into liquid ordered membrane domains. Soft Matter 2015, 11, 3241–3250. [PubMed: 25772372]

(40). DeGroot AC; Busch DJ; Hayden CC; Mihelic SA; Alpar AT; Behar M; Stachowiak JC, Entropic control of receptor recycling using engineered ligands. Biophys. J 2018, 114, 1377–1388. [PubMed: 29590595]

(41). Aguet F; Antonescu CN; Mettlen M; Schmid SL; Danuser G, Advances in analysis of low signal-to-noise images link dynamin and AP2 to the functions of an endocytic checkpoint. Dev. Cell 2013, 26, 279–291. [PubMed: 23891661]

(42). Scheve CS; Gonzales PA; Momin N; Stachowiak JC, Steric pressure between membrane-bound proteins opposes lipid phase separation. J. Am. Chem. Soc 2013, 135, 1185–1188. [PubMed: 23321000]

(43). Houser JR; Busch DJ; Bell DR; Li B; Ren P; Stachowiak JC, The impact of physiological crowding on the diffusivity of membrane bound proteins. Soft Matter 2016, 12, 2127–2134. [PubMed: 26751985]

Author Manuscript Author Manuscript Author Manuscript Author Manuscript

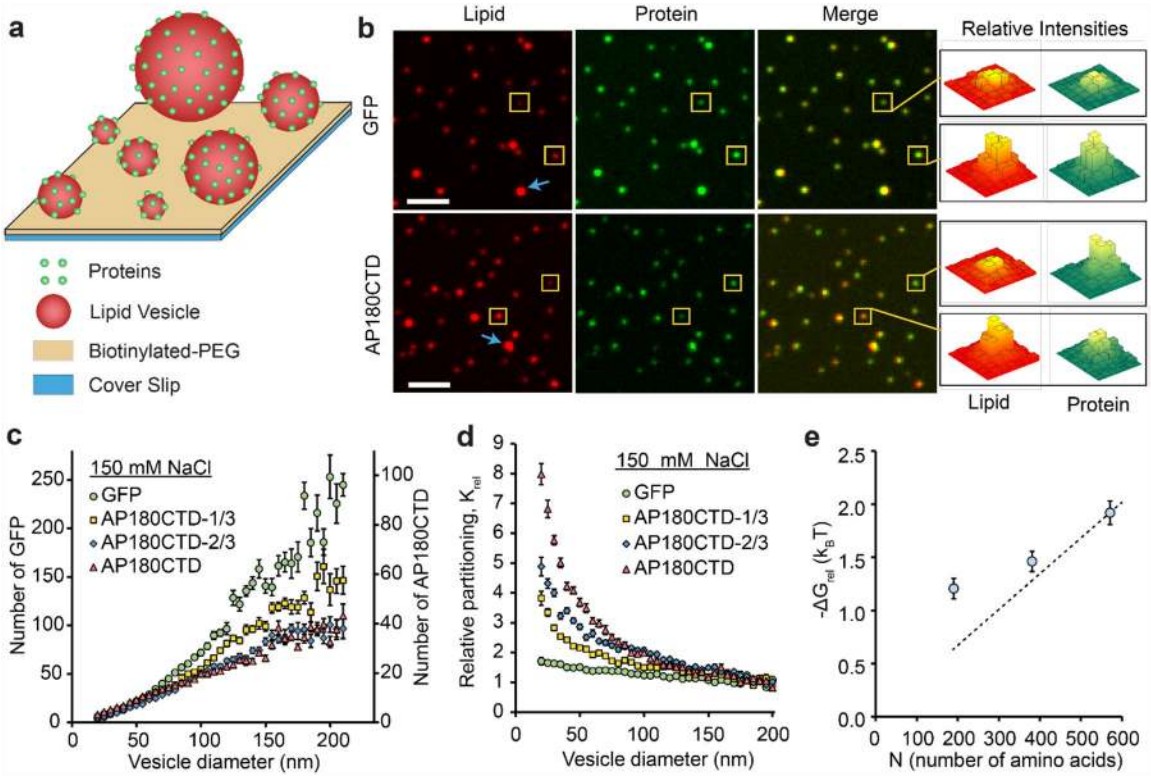

Figure 1: Amino acid chain length impacts curvature sensing by disordered proteins.

(a) Schematic of the assay used for curvature sensing. **(b)** Lipid, protein, and merged fluorescence images of extruded vesicles with either GFP or AP180CTD bound to their surfaces. Yellow boxes highlight vesicles with different fluorescent intensities, which correspond to vesicles with different diameters. Surface plots represent the distribution of pixel intensities for puncta within the yellow boxes. Vesicles contained 87.8% DOPC, 10% DGS-NTA, 2% DP-EG10-biotin, and 0.2% Texas Red-DHPE. AP180CTD truncation mutants were labeled with ATTO-488 dye. The scale bars represent 3 μm. Only diffraction limited (< 250 nm diameter) SUVs were analyzed and fit with point spread functions (see methods). Blue arrows denote representative vesicles that were not diffraction limited and therefore were not included in our analysis. **(c)** The average number of proteins bound to each vesicle as a function of vesicle diameter for populations of vesicles exposed to either GFP or one of the AP180CTD truncation mutants. **(d)** The relative partitioning of GFP and AP180CTD truncation mutants as a function of SUV diameter. **(e)** The difference in protein-membrane binding energy per protein for proteins binding to SUVs of 25 nm diameter versus proteins binding to SUVs of 200 nm diameter, as a function of the length of the AP180CTD truncation mutant. The dashed line corresponds to scaling of ΔG_{rel} predicted by polymer theory. The concentration of all proteins in **c-d** was 10 nM. Sample buffer consisted of 25 mM HEPES and 150 mM NaCl (pH = 7.4). All data in **c-d** is presented as a 5 nm-increment moving average of the raw data (>1000 data points). Each error bar represents the standard error of the mean within each bin. Each bin contains from 20–300 data points acquired cumulatively from three independent replicates. Error bars in **(e)** represent propagated errors from Equation 1.

Author Manuscript Author Manuscript Author Manuscript Author Manuscript

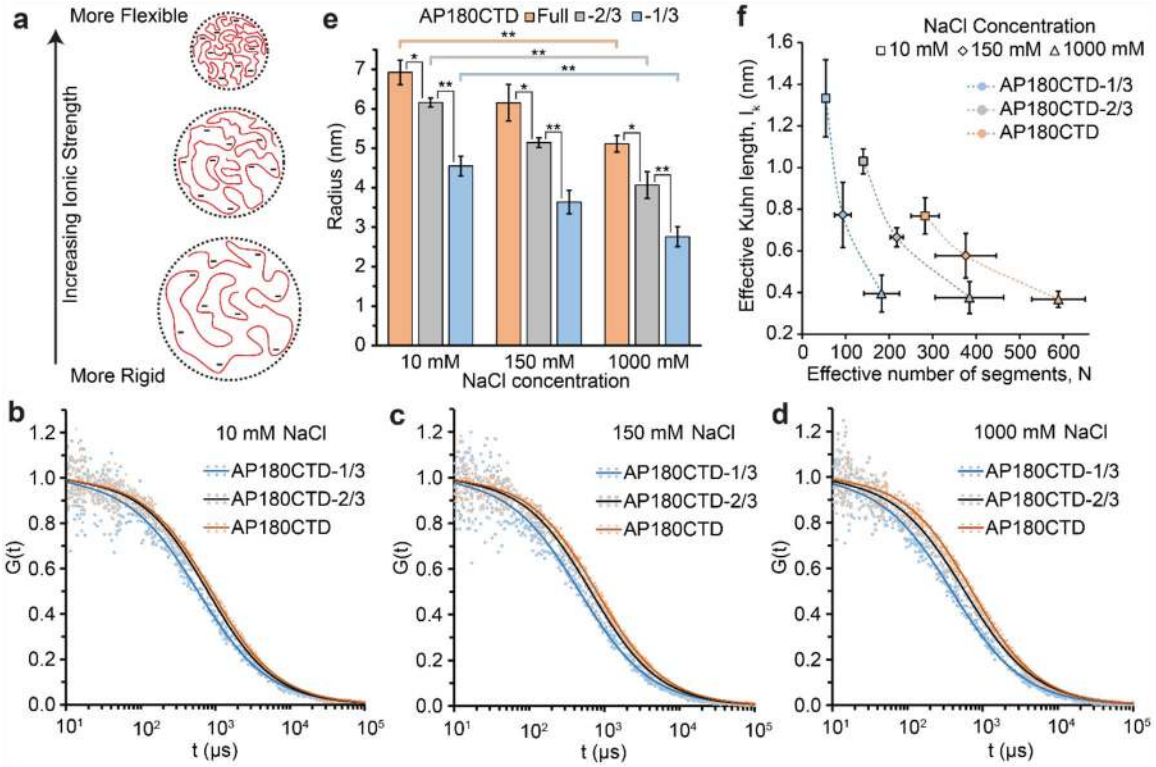

Figure 2: Ionic strength impacts the hydrodynamic radius of AP180CTD.

(a) The impact of ionic strength on chain hydrodynamic radius and flexibility. **(b-d)** Normalized correlation curves for AP180CTD truncation mutants acquired from fluorescence correlation spectroscopy (FCS). The solution buffer was held at a constant pH of 7.4 using 25 mM HEPES. The NaCl concentrations used were **(b)** 10 mM, **(c)** 150 mM, and **(d)** 1000 mM. Correlation data is represented by symbols and was acquired from three independent replicates. The best fit lines are represented by solid curves. **(e)** Estimates of the protein hydrodynamic radius based on FCS data for each of the AP180CTD truncation mutants at various sodium chloride concentrations. **(f)** Effective Kuhn Length (l_k) and number of segments (N) of AP180CTD truncation mutants for each ionic strength condition. Dashed lines in **f** serve as guides to the eye. Error bars in **e** represent the standard deviation of the mean value obtained from three independent replicates. Error bars in **f** represent the propagated errors from Supporting Equations S1 and S2. P values in **e** were calculated using unpaired, two-tailed Student's t tests.

* $P < 0.05$, ** $P < 0.01$

Author Manuscript Author Manuscript Author Manuscript Author Manuscript

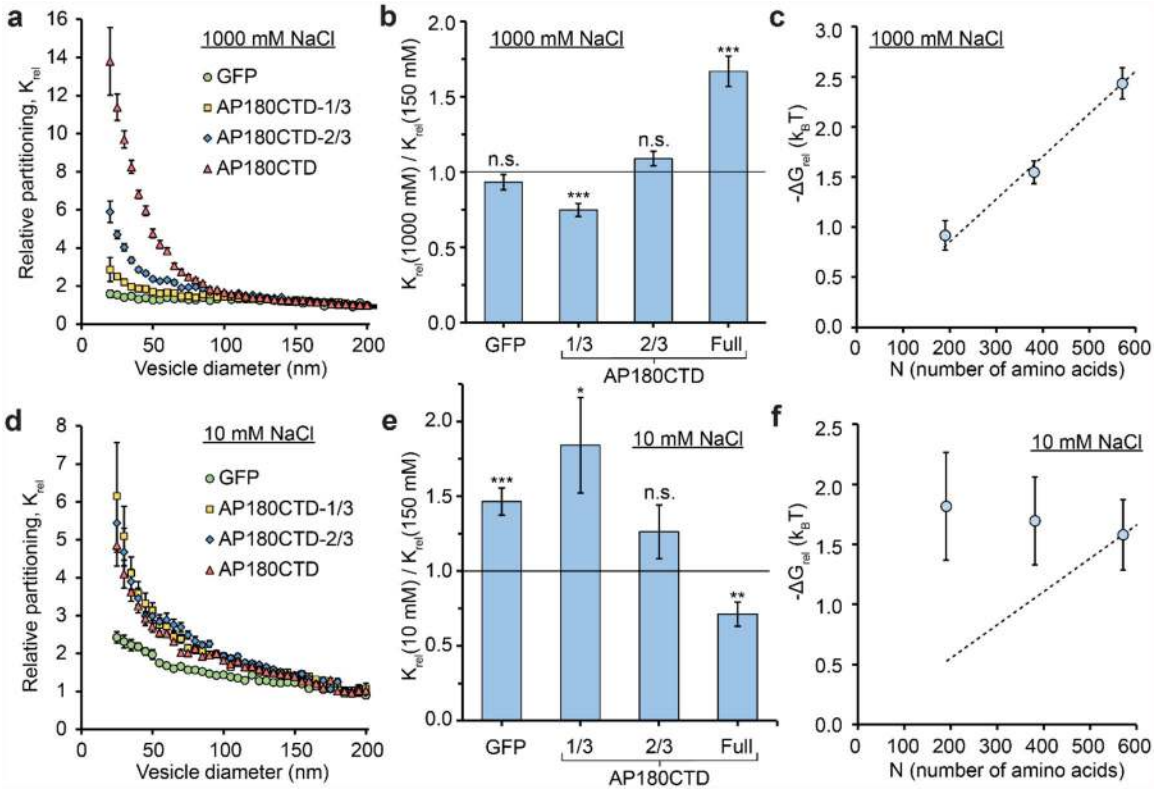

Figure 3: Ionic strength influences curvature sensing by AP180CTD.

(a) The relative partitioning of GFP and AP180CTD truncation mutants as a function of SUV diameter in buffer containing of 25 mM HEPES and 1000 mM NaCl (pH = 7.4). **(b)** The fractional change in curvature sensitivity for GFP and AP180CTD truncation mutants in buffer containing 1000 mM NaCl - K_{rel} values for 25 nm diameter SUVs in Fig. 3a (1000 mM sodium chloride) divided by K_{rel} values for 25 nm diameter SUVs in Fig. 1d (150 mM sodium chloride). **(c)** The difference in protein-membrane binding energy per protein for proteins binding to SUVs of 25 nm diameter versus proteins binding to SUVs of 200 nm diameter, as a function of the length of the AP180CTD truncation mutant. The dashed line corresponds to scaling of ΔG_{rel} predicted by polymer theory. **(d)** The relative partitioning of GFP and AP180CTD truncation mutants as a function of SUV diameter in buffer containing 25 mM HEPES and 10 mM NaCl (pH = 7.4). **(e)** The fractional change in curvature sensitivity for GFP and AP180CTD truncation mutants in buffer containing 10 mM NaCl - K_{rel} values for 25 nm diameter SUVs in Fig. 3d (10 mM sodium chloride) divided by K_{rel} values for 25 nm diameter SUVs in Fig. 1d (150 mM sodium chloride). **(f)** The difference in protein-membrane binding energy per protein for proteins binding to SUVs of 25 nm diameter versus proteins binding to SUVs of 200 nm diameter, as a function of the length of the AP180CTD truncation mutant. The dashed line corresponds to scaling of ΔG_{rel} predicted by polymer theory. All data in **a** and **d** is presented as a moving average of the raw data in 5 nm-increments (>1000 data points). Error bars in **a**, **b**, **d**, and **e** represents the standard error of the mean. Each bin in **a** and **d** contains 10–311 data points acquired cumulatively from three independent replicates. Each condition in **b** and **e** contains 25 to 311 data points. Error

bars in **c** and **f** represent propagated errors from Equation 1. P values in **b** and **d** were calculated using unpaired, two-tailed Student's t tests.
No significance = n.s, * $P < 0.05$, ** $P < 0.01$, *** $P < 0.001$

Author Manuscript Author Manuscript Author Manuscript Author Manuscript

Author Manuscript Author Manuscript Author Manuscript Author Manuscript

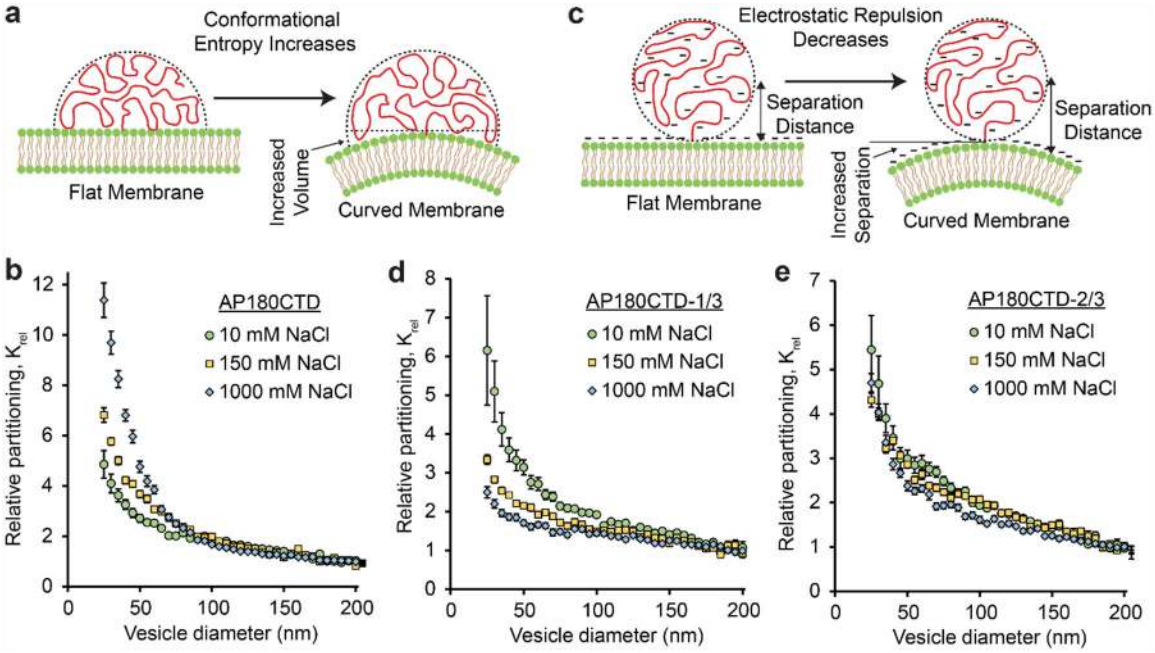

Figure 4: Curvature sensing relies on an interplay between electrostatic and entropic mechanisms.

(a) Schematic of the entropically-driven curvature sensing mechanism. **(b)** Curvature sensitivity of AP180CTD as a function of sodium chloride concentration. **(c)** Schematic of the electrostatically-driven curvature sensing mechanism. Curvature sensitivities of **(d)** AP180CTD-1/3 and **(e)** AP180CTD-2/3 as a function of sodium chloride concentration. Data in figures 4b, 4d, and 4e were replotted from figures 1d, 3a, and 3d. in the 25 to 200 nm SUV diameter range.

Author Manuscript Author Manuscript Author Manuscript Author Manuscript

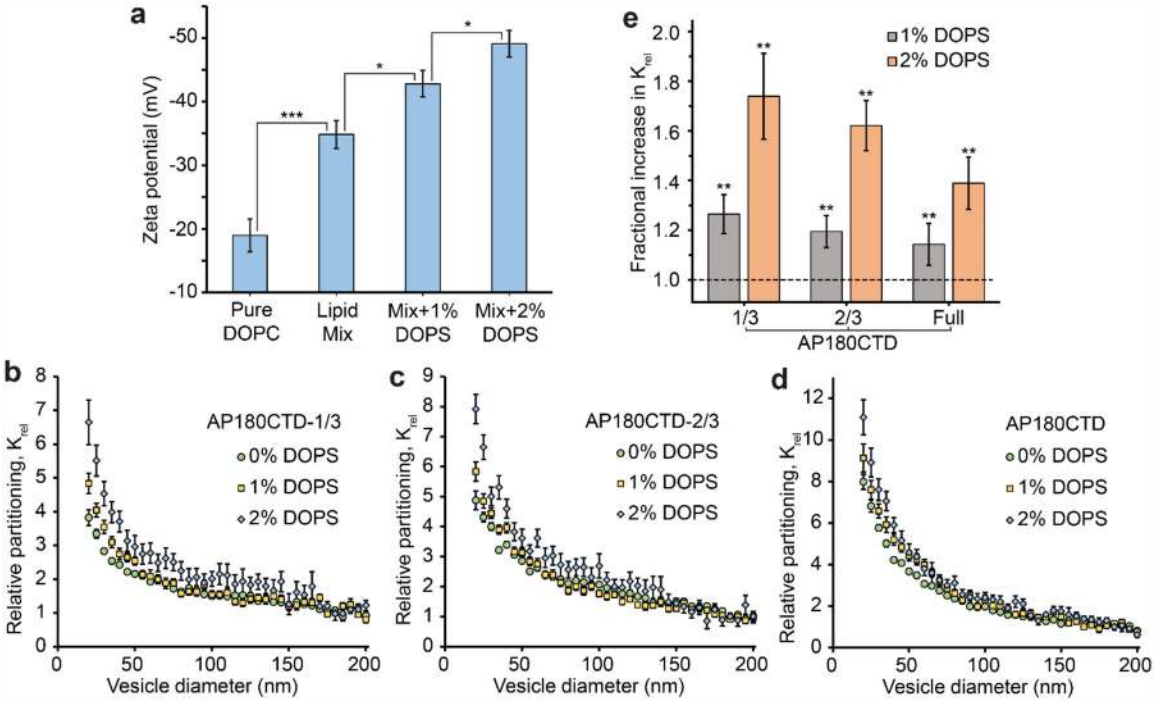

Figure 5: Curvature sensing is impacted by membrane surface potential.

(**a**) Average measured values of zeta potential for SUVs containing pure DOPC, a lipid mixture (87.8 mol% DOPC, 10 mol% DGS-NTA, 2 mol% DP-EG10-Biotin, and 0.2 mol% Texas Red-DHPE), a lipid mixture with 1% DOPS (86.8 mol% DOPC, 10 mol% DGS-NTA, 2 mol% DP-EG10-Biotin, 1 mol% DOPS, and 0.2 mol% Texas Red-DHPE), and a lipid mixture with 2% DOPS (85.8 mol% DOPC, 10 mol% DGS-NTA, 2 mol% DP-EG10-Biotin, 2 mol% DOPS, and 0.2 mol% Texas Red-DHPE). The relative partitioning of **(b)** AP180CTD-1/3, **(c)** AP180CTD-2/3, and **(d)** AP180CTD as a function of SUV diameter. SUVs contained 0–2 mol% DOPS in buffer that contained 25 mM HEPES and 150 mM NaCl (pH = 7.4). **(e)** The fractional change in curvature sensitivity for AP180CTD truncation mutants on SUVs containing either 1% or 2% DOPS - K_{rel} values for 20 nm diameter SUVs containing DOPS (Figs. 5b–d) divided by K_{rel} values for 20 nm diameter SUVs lacking DOPS (Figs. 5b–d). Error bars in **a** represent the standard error of the mean (N=36 for each condition). All data in **b**-**d** is presented as a moving average of the raw data in 5 nm increments (>1000 data points). All error bars in **b**-**e** represent the standard error of the mean within each bin. Each bin in **b**-**d** contains between 10 and 311 data points acquired cumulatively from three independent replicates. Each condition in **e** contains 98 to 198 data points. P values in **a** and **e** were calculated using unpaired, two-tailed Student's t tests.
* $P < 0.05$, ** $P < 0.01$, *** $P < 0.001$